Predictive Control Strategy for DFIG Wind Turbines with Maximum Power Point Tracking Using Multilevel Converters

José Sayritupac*, Eduardo Albánez*, Johnny Rengifo*, José M. Aller*†‡ and José Restrepo*†‡
*Universidad Simón Bolívar, Caracas–Venezuela
Email: {ealbanez,jwrengifo}@usb.ve
†PROMETEO-SENESCYT, Ecuador
‡Universidad Politécnica Salesiana, Cuenca–Ecuador
Email: jaller@ups.edu.ec

***Abstract*—This paper proposes a control scheme for a wind turbine using a DFIG electromechanical converter, implemented through an NPC three-level back to back converter, that keeps a unitary power factor injection to the grid and maximizes the energy harvested from wind, using a maximum power point tracking algorithm (MPPT). A predictive direct power control (DPC) strategy drives the grid-side converter, to maintain the DC bus reference voltage. Whereas, a predictive direct torque control (DTC) strategy drives the machine-rotor-side converter, to control the power extraction, the power factor and balancing of the DC bus capacitors. The developed model allows to study the wind energy conversion system (WECS) for energy harvesting, rotor dynamics and power quality analysis. Simulation results endorse the effectiveness of the advanced control techniques for the whole wind spectrum, including the pitch angle control. A sensitivity analysis shows that the predictive DTC control strategy is robust with an uncertainty up to 20% of the induction machine parameters.**

***Index Terms*—WECS, DFIG, DTC, DPC, Predictive control**

NOMENCLATURE

θ_e	Electrical angle among rotor & stator α-axis
$\theta_{p,0}$	Blade pitch angle
ρ	Air density
ρ_T, ρ_λ, ρ_v	DTC cost function weights
ρ_p, ρ_q	DPC cost function weights
φ	Angle of relative wind
Λ	Tip speed ratio
Λ_h	Tip speed ratio at the hub
Λ_r	Tip speed ratio at a distance r from the hub
ω_m	Generator shaft angular speed
ω_t	Turbine rotor angular speed
ω_e	Electric system synchronous speed
a, a'	Axial and angular induction factors
a_{gb}	Gear box transformation ratio
A	Area swept by the turbine rotor
C	Capacitance of each DC bus capacitors
C_D	Airfoil drag coefficient
C_L	Airfoil lift coefficient
C_p	Turbine power coefficient
i_{ra}, i_{rb}, i_{rc}	Phase rotor currents
i_{ga}, i_{gb}, i_{gc}	Phase grid side currents
J	Moment of inertia
L_s, L_r, L_{sr}	Stator, rotor and mutual inductances
n_p	Number of pole pairs
p	Derivative operator $^d/_{dt}$
R	Turbine rotor radius
R_s, R_r	Stator and rotor resistances
R_g, L_g	Transformer resistance and inductance
S_a, S_b, S_c	Bridge leg states
S_w	Switching state vector
T_e, T_m	Electrical and mechanical torque
T_s	Sampling time
$\vec{v}_s$, $\vec{i}_s$	Stator voltage and current space vectors

I. INTRODUCTION

There is a great interest in the scientific community on researching wind energy conversion systems (WECS), due to its sustained growing inclusion in electric power systems in the last decades [1]. Doubly fed induction generators (DFIG) are the most installed technology used to exploit the wind energy resources [2], mainly because the rated power of the electronic converter is a third of the induction generator capacity.

Several strategies based on direct torque control (DTC) [3] have been proposed in recent years, including predictive control and multilevel converters [4]–[6]. Some DFIG applications are reported in [1], [7]–[9]. Maximum power point tracking (MPPT) algorithms have been presented [10], [11] in order to optimize the energy extraction from the wind.

This paper presents a WECS based on a DFIG topology controlled by a back to back power converter, build upon two three-level neutral point clamped (NPC) bridges linked by a DC bus. The machine-side converter is controlled with the proposed DTC technique, and the grid-side converter use a direct power control (DPC) strategy proposed by [12]. Both controls minimize cost functions based on the control variables errors at every control cycle to select the switching states of each converter. The DPC references are set to keep constant the DC bus voltage, whereas the DTC references are set to maximize

the power extraction from the wind, control the stator power factor and guarantee the balance of DC bus capacitors. The torque reference is established by a maximum power point tracking (MPPT) algorithm, that takes into account the blade pitch angle. The WECS model developed allows to study the rotor dynamics, power quality analysis, and control strategies for different wind turbine models.

II. Wind Energy Conversion System

The wind energy conversion system studied on this paper is shown in Fig. 1.

A. Wind speed

A wind speed measurement that includes wind gust and a wind ramp was obtained from [13], and provides a global scenario suitable to analyze the energy conversion system dynamics and the performance of the control strategies.

B. Wind turbine

The torque developed by the turbine rotor is [14], [15],

$$T_m = \frac{P_m}{\omega_t} = \frac{\rho A V^3}{2\omega_t} C_p\left(\Lambda, \theta_{p,0}\right) \tag{1}$$

where the power coefficient in accordance with the Blade Element Momentum Theory is expressed as [16],

$$C_p = \frac{8}{\Lambda}\int_{\Lambda_h}^{\Lambda} \Lambda_r^3 a'\left(1-a\right)\left(1-\frac{C_D}{C_L}\cot\varphi\right) d\Lambda_r \tag{2}$$

The power coefficient surface, as a function of the the tip speed ratio and the pitch angle, for the data shown in appendix A, is depicted in Fig. 2.

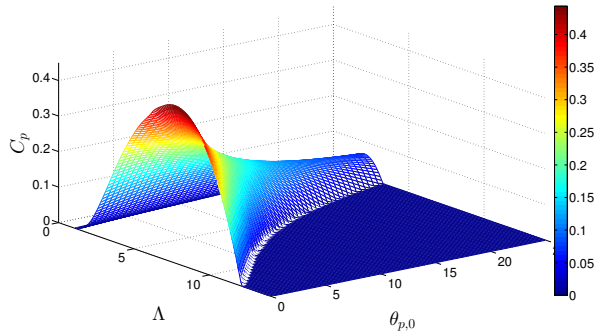

Figure 2: C_p vs λ curves.

C. Doubly fed induction generator

The fixed stator reference frame $\alpha\beta$ space vector model of the induction machine is [17],

$$\vec{v}_s = R_s\vec{i}_s + L_s p\vec{i}_s + L_{sr} p\vec{i}_r^s \tag{3}$$

$$\vec{v}_r^s = R_r\vec{i}_r^s + L_{sr} p\vec{i}_s + L_r p\vec{i}_r^s - j n_p\omega_m\left(L_{sr}\vec{i}_s + L_r\vec{i}_r^s\right) \tag{4}$$

$$J\, p\omega_m = T_e - T_m = n_p L_{sr}\left(\vec{i}_r^s \times \vec{i}_s\right) - T_m \tag{5}$$

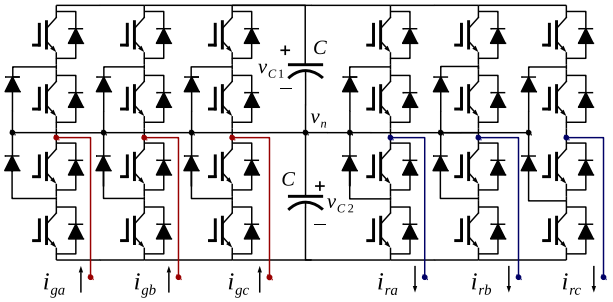

Figure 3: Back to back NPC three level converter

$$p\theta_e = n_p\omega_m \tag{6}$$

The space-vector transformation used in this paper is,

$$\vec{x} = \sqrt{\frac{2}{3}}\left(x_a + x_b e^{j\frac{2\pi}{3}} + x_c e^{j\frac{4\pi}{3}}\right) = x_\alpha + j x_\beta \tag{7}$$

and the transformation to refer to the rotor variables to the frame of reference fixed in the stator is,

$$\vec{x}_r^s = \vec{x}_r e^{j\theta_e} \tag{8}$$

D. Multilevel back to back converter

The back to back converter is shown in Fig. 3. Each inverter generates $3^3 = 27$ different valid voltage space vectors in the $\alpha\beta$ reference frame. The switching variable $S_w = [S_a,\, S_b,\, S_c]^t$ denotes the converter switching position for each leg, these integer variables are -1, 0 or 1 corresponding to the phase voltages $-\frac{V_{dc}}{2}$, 0, $\frac{V_{dc}}{2}$.

The NPC topology requires to keep the voltage on each capacitor equal, but these voltages are affected by the connectivity states when S_a, S_b or S_c are zero [18]. The strategy for balance operation consists in controlling the neutral voltage v_n around zero volts. The dynamic response of v_n is described by [19],

$$p v_n = \frac{1}{C}\sum_{m=\{a,b,c\}} |S_{gm}|\, i_{gm} - |S_{rm}|\, i_{rm} \tag{9}$$

III. Control Strategies

A. Predictive direct power control

The predictive DPC presented in [12], [20] proposes an algorithm for computing the optimum voltage space vector that satisfies the active and reactive power references [21]. This formulation is based on computing the optimum trajectory using Lagrange operators. The system voltage may be expressed as a function of the grid-side converter voltage as,

$$\vec{v}_{sys} = R_g\vec{i}_g + L_g p\vec{i}_g + \vec{v}_g \tag{10}$$

Using a first order approximation, an expression for the increment of the apparent power for each control cycle k is,

$$\Delta\vec{s}_k = \Delta p_k + j\Delta q_k \tag{11}$$

$$\Delta\vec{s}_k = \Delta\vec{s}_{0,k} - \frac{T_s}{L_g}\left(\vec{v}_{sys,k+1}\,\vec{v}_{g,k}^{\,*}\right) \tag{12}$$

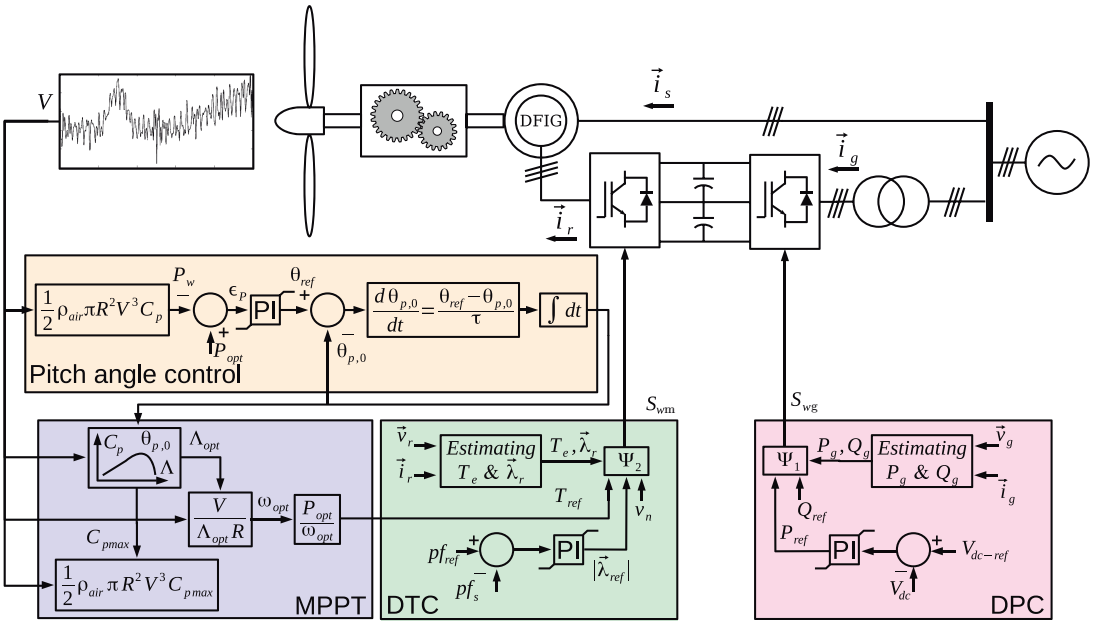

Figure 1: WECS topology and system control block diagrams.

$$\Delta\vec{s}_{0,k} = \Delta\vec{v}_{sys,k}\,\vec{i}_g^{*} + \vec{v}_{sys,k+1}\,\frac{T_s}{L_g}\left(\vec{v}_{sys,k} - R_g\vec{i}_{g,k}\right)^{*} \quad (13)$$

where the electric system voltage $\vec{v}_{sys,k}$ is sinusoidal, and the estimated voltage for the next control cycle $\vec{v}_{sys,k+1}$ is obtained by rotating $\vec{v}_{sys,k}$

$$\vec{v}_{sys,k+1} = \vec{v}_{sys,k}e^{j\omega_e T_s} \quad (14)$$
$$\Delta\vec{v}_{sys,k} = \vec{v}_{sys,k}\left(e^{j\omega_e T_s} - 1\right)$$

Given an active and reactive power references, the errors are defined as,

$$\epsilon_k = \epsilon_{p,k} + j\epsilon_{q,k} = (p_{ref,k+1} - p_k) + j\,(q_{ref,k+1} - q_k) \quad (15)$$

The cost function Ψ_1 follows as,

$$\Psi_1 = \rho_p\,(\epsilon_{p,k} - \Delta p_k)^2 + \rho_q\,(\epsilon_{q,k} - \Delta q_k)^2 \quad (16)$$

B. Predictive direct torque control

The predictive strategy is based on applying the optimal rotor voltage space vector $\vec{v}_r$ that best accomplishes the following targets:

1) Maximize the energy harvested from wind, through the torque reference obtained from the MPPT algorithm.
2) Control the stator power factor, using a closed-loop PI controller to set the flux reference.
3) Balance each capacitor voltage of the DC bus, by computing the $\vec{v}_r$ using redundant switching states of the back to back converter when possible.

The selection of $\vec{v}_r$ is performed by minimizing a cost function that takes into account the electric torque, the rotor flux magnitude and the neutral point voltage of the DC bus, at the next control cycle.

The discrete-time form of the estimated torque is,

$$T_{e,k+1} = T_{e,k} + \Delta T_{e,k} \quad (17)$$

Differentiating the electric torque in (5) leads to,

$$\Delta T_e = T_s n_p L_{sr}\left(p\vec{i}_{r,k}\times\vec{i}^{\,r}_{s,k} + \vec{i}_{r,k}\times p\vec{i}^{\,r}_{s,k}\right) \quad (18)$$

Replacing $p\vec{i}^{\,r}_s$ and $p\vec{i}_r$ from (3) and (4) respectively, in (18), the following expression for the change of the electric torque is obtained,

$$\begin{aligned}\Delta T_{e,\vec{v}_s} = -T_s\frac{n_p L_{sr}}{L_s L_r - L_{sr}^2}\Big[&\vec{v}^{\,r}_{s,k}\times\left(L_{sr}\vec{i}^{\,r}_{s,k} + L_r\vec{i}_{r,k}\right) + \\ &(L_s R_r + L_r R_s)\left(\vec{i}_{r,k}\times\vec{i}^{\,r}_{s,k}\right) + \\ &\omega_m L_{sr}\left(L_s|\vec{i}^{\,r}_{s,k}|^2 + L_r|\vec{i}_{r,k}|^2\right) + \\ &\omega_m\left(L_s L_r + L_{sr}^2\right)\Re_e\left\{\vec{i}_{r,k}\vec{i}^{\,r}_{s,k}\right\}\Big]\end{aligned} \quad (19)$$

$$\Delta T_{e,\vec{v}_r} = T_s\frac{n_p L_{sr}}{L_s L_r - L_{sr}^2}\left[\vec{v}_{r,k}\times\left(L_s\vec{i}^{\,r}_{s,k} + L_{sr}\vec{i}_{r,k}\right)\right] \quad (20)$$

with,

$$\Delta T_e = \Delta T_{e,\vec{v}_s} + \Delta T_{e,\vec{v}_r} \quad (21)$$

The discrete-time form of the estimated rotor flux amplitude is,

$$\left|\vec{\lambda}_{r,k+1}\right| = \left|\vec{\lambda}_{r,k}\right| + \Delta\left|\vec{\lambda}_{r,k}\right| \quad (22)$$

the rotor voltage equation is,

$$p\vec{\lambda}_r = \vec{v}_r - R_r\vec{i}_r \tag{23}$$

$$p\left|\vec{\lambda}_{r,k}\right| = \frac{\Re_e\left(\vec{\lambda}_{r,k}\left(\vec{v}_{r,k} - R_r\vec{i}_{r,k}\right)\right)}{\left|\vec{\lambda}_{r,k}\right|}$$

then,

$$\Delta\lambda_{r,k} = T_s\frac{\Re_e\left(\vec{\lambda}_{r,k}\left(\vec{v}_{r,k} - R_r\vec{i}_{r,k}\right)\right)}{\left|\vec{\lambda}_{r,k}\right|} \tag{24}$$

The change of the neutral voltage of the DC bus from (9) is,

$$\Delta v_{n,k} = \frac{T_s}{C}\sum_{m=\{a,b,c\}}|S_{gm,k}|\,i_{gm,k} - |S_{rm,k}|\,i_{rm,k} \tag{25}$$

The electric torque, rotor flux and neutral point voltage errors are defined as,

$$\epsilon_T = T_{ref} - T_{e,k}\,;\ \epsilon_\lambda = \lambda_{ref} - \left|\vec{\lambda}_{r,k}\right|\ ;\ \epsilon_v = v_{ref} - v_{n,k} \tag{26}$$

The cost function Ψ_2 used in this work is,

$$\Psi_2 = \rho_T\left(\epsilon_{T,k} - \Delta T_{e,k}\right)^2 + \rho_\lambda\left(\epsilon_{\lambda,k} - \Delta\lambda_{r,k}\right)^2 \ldots + \rho_v\left(\epsilon_{v,k} - \Delta v_{n,k}\right)^2 \tag{27}$$

C. Maximum power point tracking

The wind turbine has an optimum operating point $(C_{p-opt}, \lambda_{opt})$ for a given pitch angle $\theta_{p,0}$ and wind speed V, as depicted in Fig. 4, where the the power P_{m-opt} captured from the wind is maximum,

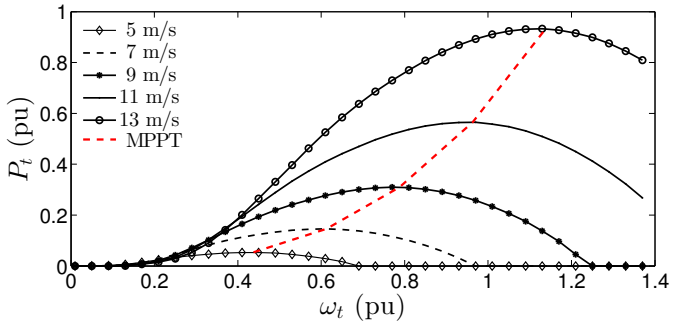

Figure 4: Wind turbine power extraction vs angular mechanical speed, for a fixed pitch angle.

$$P_{m-opt} = \frac{1}{2}\rho A V^3 C_{p-opt} \tag{28}$$

$$\omega_{t-opt} = \frac{V}{R}\lambda_{opt} \tag{29}$$

then the torque reference for the DTC is,

$$T_{ref} = \frac{P_{m-opt}}{a_{gb}\omega_{t-opt}} \tag{30}$$

D. Pitch control

For wind speeds exceeding the turbine rated value, the blades pitch angle can be controlled to maintain the generator power at its rated capacity. The pitch angle model can be expressed as [22], [23],

$$p\theta_{p,0} = \frac{\theta_{ref} - \theta_{p,0}}{\tau_\theta} \tag{31}$$

where τ_θ represents the mechanical servomotor time delay. The angle θ_{ref} is set to zero when the wind speed is below its rated value, otherwise the reference is obtained from a PI controller to keep the generator operating at rated power.

IV. Simulation Results

A detailed analysis of the WECS to evaluate the performance of the proposed control strategy is presented, the simulation data is given in Appendix A. All per units results presented in this section are based on the generator rated values.

A. Case of study

The system dynamics are studied within a $50\,\mathrm{s}$ window of incident wind speed. The power delivered to the electric grid varies accordingly with the wind fluctuations as shown in Fig. 5a. The turbine power is effectively limited to its rated value when the wind gust ($12\,\mathrm{s} < t < 17\,\mathrm{s}$) and the wind ramp ($t > 39\,\mathrm{s}$) take place, as a result of the active blade pitch angle control. When the wind speed is under its rated value the pitch angle is set to zero, and the DTC shows a fast response to the MPPT reference, to keep the optimum turbine power coefficient of 0.42. As the wind speed exceeds its rated value of $12\,{}^{m}\!/\!_{s}$, the pitch angle grows reducing the C_p accordingly to Fig. 5b. When the power coefficient differs from zero, the trajectory followed by it, is the crest of the surface depicted in Fig. 2.

The DPC holds the DC bus voltage at its reference value of $3\,\mathrm{pu}$, whereas the DTC maintains the capacitors voltage balanced at $1.5\,\mathrm{pu}$ each, as shown in Fig. 6. The rotor flux linkage was set to keep a lagging power factor of 0.95 at the electric generator terminals. Table I synthesizes these results. The variation of the turbine mechanical speed is presented in Fig. 7, which varies slowly due to its large inertial time constant. Lastly, the phase current detail and its frequency spectrum is depicted Fig. 8, in which the signal harmonic content is kept 40 decades below the fundamental frequency until the 49^{th} harmonic.

Table I: Power factor results

Mean	Median	Standard deviation
0.9455	0.9568	0.0454

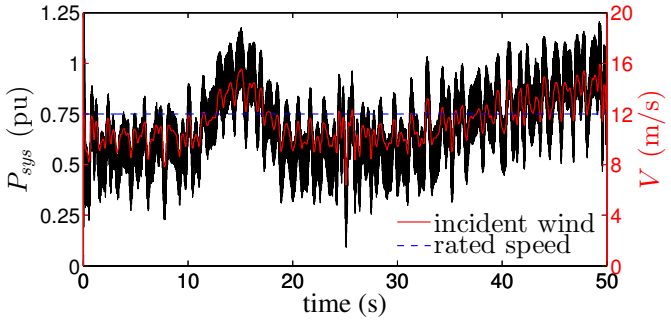

(a) Active power delivered and incident wind speed

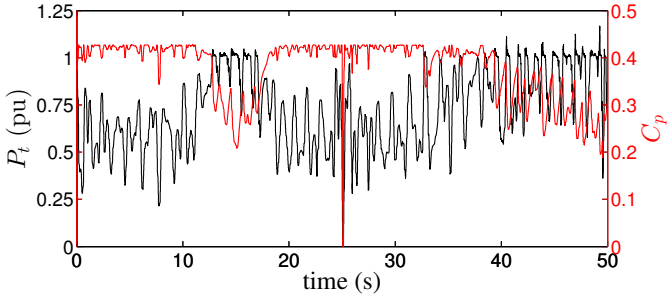

(b) Turbine power and power coefficient

Figure 5: WECS performance during the study case

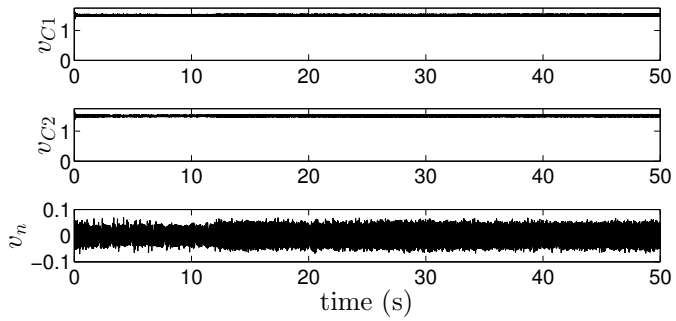

Figure 6: Capacitors and neutral DC voltages

B. *Sensitivity analysis*

The proposed DTC strategy requires knowledge of the machine parameters to predict the optimum operating point at the next control cycle. Therefore, is of interest to assess the robustness of the control under parameter detuning conditions. To this purpose, the algorithm was tested varying each parameter over a range of $\pm 20\%$. The variable σ_T is define in (32) to quantify the torque ripple. The results of the sensitivity analysis are presented in Table II, where the control scheme exhibits a primary dependency with L_{sr}. For the worst case scenario considered, the torque ripple is kept below 3.5%.

$$\sigma_T = 100\,\frac{1}{N_i}\sum_{k=1}^{N_i}\frac{1}{T_{ref,k}}\sqrt{\left(T_{ref,k}-T_{e,k}\right)^2} \qquad (32)$$

V. Conclusion

A DFIG-based wind energy conversion system has been simulated, using a detailed model of the turbine operating under demanding wind speed conditions. The proposed DTC strategy is applied using a three-level NPC converter to control the electric generator has proven to be effective, with a fast tracking MPPT reference that maximizes the harvesting of the wind energy; greatly reducing the reactive power requirements by keeping the power factor close to unity; and balancing the voltage of the back to back converter DC bus capacitors.

The proposed control technique was tested for machine-parameters detuning, revealing a main dependence with the mutual inductance. In spite of this, the sensitivity analysis showed the robustness of the DTC under this operating con-

Table II: Torque ripple under parameters uncertainty

	R_s	R_r	$L_{\sigma s}$	$L_{\sigma r}$	L_{sr}
$+20\%$	1.5476	1.5476	1.7532	1.7699	3.5431
0%			1.5474		
-20%	1.5483	1.5434	1.5229	1.5287	3.2035

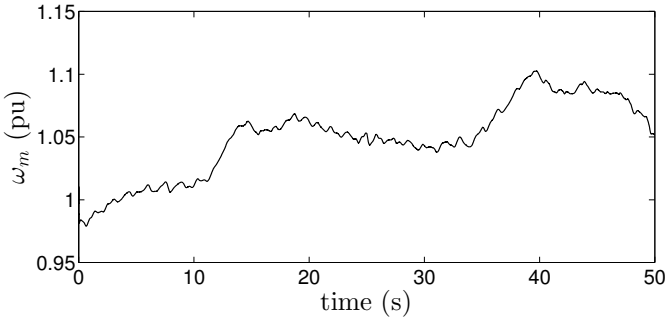

Figure 7: Angular mechanical speed

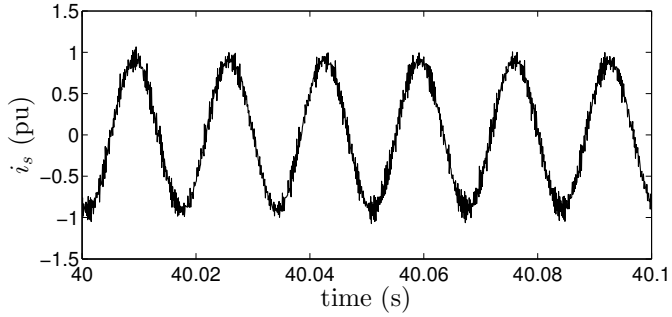

(a) Detail of stator phase current

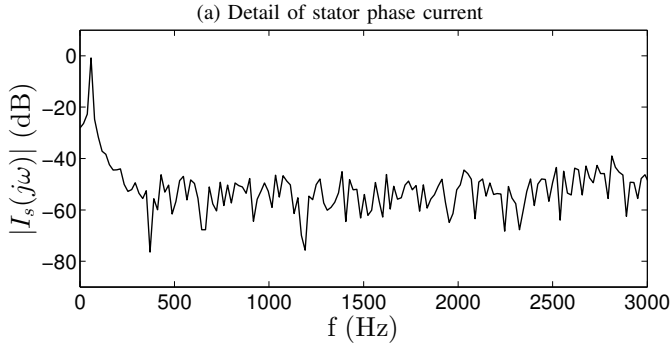

(b) Frequency spectrum of the stator current

Figure 8: Analysis of the stator phase current

dition.

ACKNOWLEDGMENT

The authors gratefully acknowledge the support of Prometeo Project, Secretaría de Educación Superior, Ciencia, Tecnología e Innovación, and Universidad Politécnica Salesiana, both in República del Ecuador, as well as Universidad Simón Bolívar and FONACIT Research Project #2011000970 both in Venezuela.

REFERENCES

[1] J. Liang, D. Howard, J. Restrepo, and R. Harley, "Feedforward transient compensation control for dfig wind turbines during both balanced and unbalanced grid disturbances," *Industry Applications, IEEE Transactions on*, vol. 49, no. 3, pp. 1452–1463, May 2013.

[2] Z. Zhang, A. Matveev, S. Ovrebo, R. Nilssen, and A. Nysveen, "State of the art in generator technology for offshore wind energy conversion systems," in *Electric Machines Drives Conference (IEMDC), 2011 IEEE International*, May 2011, pp. 1131–1136.

[3] I. Takahashi and T. Noguchi, "A new quick-response and high-efficiency control strategy of an induction motor," *Industry Applications, IEEE Transactions on*, vol. IA-22, no. 5, pp. 820–827, Sept 1986.

[4] T. Geyer, G. Papafotiou, and M. Morari, "Model predictive direct torque control part i: Concept, algorithm, and analysis," *Industrial Electronics, IEEE Transactions on*, vol. 56, no. 6, pp. 1894–1905, June 2009.

[5] G. Papafotiou, J. Kley, K. Papadopoulos, P. Bohren, and M. Morari, "Model predictive direct torque control part ii: Implementation and experimental evaluation," *Industrial Electronics, IEEE Transactions on*, vol. 56, no. 6, pp. 1906–1915, June 2009.

[6] J. Rengifo, J. Aller, A. Berzoy, and J. Restrepo, "Predictive dtc algorithm for induction machines using sliding horizon prediction," in *Circuits and Systems (LASCAS), 2014 IEEE 5th Latin American Symposium on*, Feb 2014, pp. 1–4.

[7] L. Xu and P. Cartwright, "Direct active and reactive power control of dfig for wind energy generation," *Energy Conversion, IEEE Transactions on*, vol. 21, no. 3, pp. 750–758, Sept 2006.

[8] G. Abad, M. Rodriguez, and J. Poza, "Two-level vsc-based predictive direct power control of the doubly fed induction machine with reduced power ripple at low constant switching frequency," *Energy Conversion, IEEE Transactions on*, vol. 23, no. 2, pp. 570–580, June 2008.

[9] J. Mohammadi, S. Vaez-Zadeh, S. Afsharnia, and E. Daryabeigi, "A combined vector and direct power control for dfig-based wind turbines," *Sustainable Energy, IEEE Transactions on*, vol. 5, no. 3, pp. 767–775, July 2014.

[10] M. Abdullah, A. Yatim, C. Tan, and R. Saidur, "A review of maximum power point tracking algorithms for wind energy systems," *Renewable and Sustainable Energy Reviews*, vol. 16, no. 5, pp. 3220–3227, 2012.

[11] Y. Xia, K. Ahmed, and B. Williams, "Wind turbine power coefficient analysis of a new maximum power point tracking technique," *Industrial Electronics, IEEE Transactions on*, vol. 60, no. 3, pp. 1122–1132, March 2013.

[12] J. Restrepo, J. Aller, J. Viola, A. Bueno, and T. Habetler, "Optimum space vector computation technique for direct power control," *Power Electronics, IEEE Transactions on*, vol. 24, no. 6, pp. 1637–1645, June 2009.

[13] Slootweg, J.G., "Wind power: Modelling and impact on power system dynamics," Ph.D Dissertation, Delft University of Technology, Delft, Netherlands, 2003.

[14] T. Burton, D. Sharpe, N. Jenkins, and E. Bossanyi, *Wind energy handbook*. John Wiley & Sons, 2001.

[15] I. Munteanu, A. I. Bratcu, N.-A. Cutululis, and E. Ceanga, *Optimal control of wind energy systems: towards a global approach*. Springer Science & Business Media, 2008.

[16] J. F. Manwell, J. G. McGowan, and A. L. Rogers, *Wind energy explained: theory, design and application*, 2nd ed. Chichester, U.K.: Wiley, 2009.

[17] P. C. Krause, O. Wasynczuk, S. D. Sudhoff, and S. Pekarek, *Analysis of electric machinery and drive systems*. John Wiley & Sons, 2013, vol. 75.

[18] N. Celanovic and D. Boroyevich, "A comprehensive study of neutral-point voltage balancing problem in three-level neutral-point-clamped voltage source pwm inverters," *Power Electronics, IEEE Transactions on*, vol. 15, no. 2, pp. 242–249, Mar 2000.

[19] H. du Toit Mouton, "Natural balancing of three-level neutral-point-clamped pwm inverters," *Industrial Electronics, IEEE Transactions on*, vol. 49, no. 5, pp. 1017–1025, Oct 2002.

[20] J. Restrepo, J. Viola, J. Aller, and A. Bueno, "Algorithm evaluation for the optimal selection of the space vector voltage using dpc in power systems," in *Power Electronics and Applications, 2007 European Conference on*, Sept 2007, pp. 1–9.

[21] J. Aller, A. Bueno, J. Restrepo, M. Gimenez de Guzman, and V. Guzman, "Advantages of the instantaneous reactive power definitions in three phase system measurement," *Power Engineering Review, IEEE*, vol. 19, no. 6, pp. 54–56, Jun 1999.

[22] L. Yang, Z. Xu, J. Ostergaard, Z. Y. Dong, K. P. Wong, and X. Ma, "Oscillatory stability and eigenvalue sensitivity analysis of a dfig wind turbine system," *Energy Conversion, IEEE Transactions on*, vol. 26, no. 1, pp. 328–339, March 2011.

[23] M. Zamanifar, B. Fani, M. Golshan, and H. Karshenas, "Dynamic modeling and optimal control of dfig wind energy systems using dft and nsga-ii," *Electric Power Systems Research*, vol. 108, pp. 50–58, 2014.

APPENDIX A
AERODYNAMIC DATA

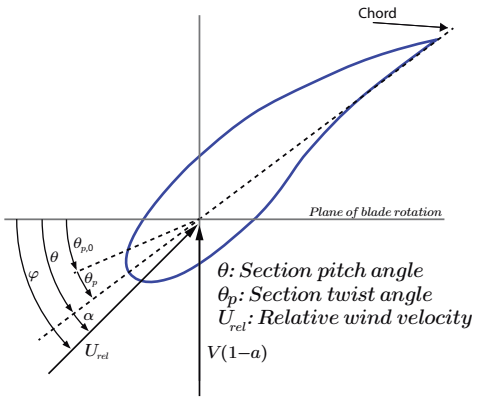

Figure 9: Airfoil aerodynamics..

Table III: Simulation data

Specification	Variable	Value	Unit
Turbine rated power	-	1	MW
Rated wind speed	-	12	m/s
Inertia time constant	H_t	4	s
Turbine rotor radius	R	26	m
Gear box transformation ratio	a_{gb}	65	-
Servomotor time delay	τ_θ	0.25	s
Number of blades		3	
Blade model		LM-26	
Generator rated power		1	MW
Stator resistance	R_e	0.0108	pu
Rotor resistance	R_r	0.0121	pu
Stator inductance	L_s	3.4640	pu
Rotor inductance	L_r	3.4720	pu
Mutual inductance	L_{er}	3.3620	pu
Stator rated voltage	-	575	V
Rotor rated voltage	-	1975	V
Capacitance of each capacitor	C	2	pu
Reference DC voltage	-	3	pu
Converter switching frequency	-	10	kHz
Transformer resistance	R_g	0.01	pu
Transformer leakage inductace	L_g	0.2	pu